Effect of configuration mixing on $3d$-$4f$ transitions in highly ionized Ga-, Zn-, and Cu-like ions

P. Mandelbaum* and J. F. Seely
E. O. Hulburt Center for Space Research, Naval Research Laboratory, Washington, D.C. 20375-5000

A. Bar-Shalom
Nuclear Research Center of the Negev, P.O. Box 9001, Beer Sheva, Israel

M. Klapisch
Lawrence Berkeley Laboratory, Berkeley, California 94720
(Received 28 May 1991)

It is shown that the introduction of configuration interaction through $4s4f$-$4p4d$ and $4p4f$-$4d^2$ mixing has a very significant effect on $3d$-$4f$ transitions in highly charged Ga-, Zn-, and Cu-like ions. This effect changes the width and, to a lesser extent, the mean wavelength of transition arrays as compared to the spin-orbit split array model. Because of this mixing, lines previously identified as dielectronic recombination satellites may have a non-negligible inner-shell excitation component. This should be taken into account in models for the intensities of these lines.

PACS number(s): 31.20.Tz, 32.30.Rj, 52.25.Nr

I. INTRODUCTION

Many spectra of highly ionized elements emitted from laboratory plasmas are characterized by strong $3d$-$4f$ emission from ions neighboring the Ni-like charge state (ground-state $3d^{10}$ and transitions $3d^{10}$-$3d^9 4f$). Laser-produced-plasma spectra of many high-Z elements showing these features have been published (see Ref. [1] and references therein). A typical spectrum emitted from a laser-produced tantalum plasma is shown in Fig. 1. This spectrum, obtained at the Soreq Nuclear Center has already been analyzed in Ref. [1] where details on the experimental setup and wavelength calibration can be found. For this kind of spectrum, the only theoretical means for transition identification is *ab initio* accurate predictions together with careful isoelectronic sequence considerations. Indeed, the classical method of parametric fitting of level energies cannot be applied for such high-ionization stages, since blending of lines is the rule, and most of the features appearing in the spectra are unresolved transition arrays (UTA's). This was pointed out by Wyart *et al.* [2] in the case of the Cu-like $3d$-$4p$ sequence. The analysis of the $3d$-$4f$ pseudocontinuum was first performed by Klapisch *et al.* [1] for the spectra of Tm to Re and by Busquet *et al.* [3] for the Au spectrum. The two latter works rely on computations using the RELAC code based on the relativistic parametric potential method [4]. Because of the nature of the spectrum, with a very large number of lines merging into unresolved transition arrays, extensive use of the spin-orbit split array (SOSA) [5] model was made by Klapisch *et al* [1]. The SOSA model is a version of the UTA theory [6] that accounts for the splitting of the array into jj components. However, some discrepancies inherent to the SOSA approximation were found in Ref. [1]. The origin of these discrepancies is twofold.

(i) The SOSA model as used in Ref. [1] assumed pure jj coupling. It was found that, even if the $3d$-$4f$ array was conspicuously split into subarrays corresponding to the different $3d$-$4f$-allowed jj transitions, some residual interaction between the relativistic subconfigurations gave additional wavelength shifts and redistribution of intensities that was not taken into account in the SOSA model. Recently, the global effects of the mixing of relativistic subconfigurations (the breakdown of jj coupling) on the intensities of the SOSA subarrays has been included in

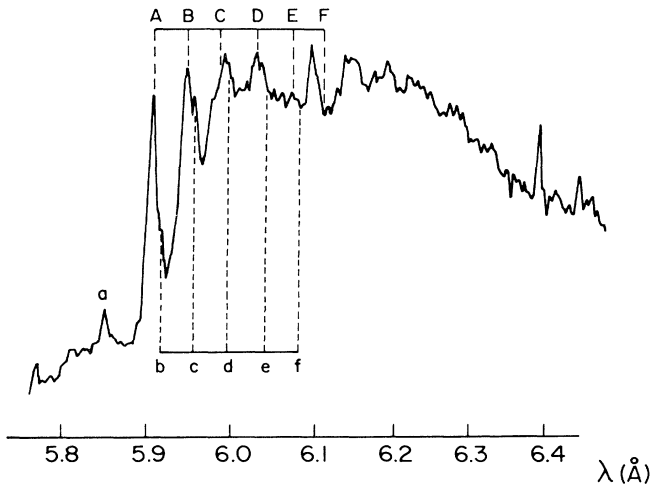

FIG. 1. Spectrum of tantalum emitted from a laser-produced plasma in the 5.8–6.4-Å region (courtesy of Dr. A. Zigler). $A,B,C,\ldots$:$3d_{3/2}$-$4f_{5/2}$ transition in Ni-, Cu-, Zn-,... like tantalum with the $4l$ spectator electron. $b,c,d,\ldots$, same as $B,C,D,\ldots$, but among the spectator electrons, one belongs to $5l$ (see Ref. [15]).

the SOSA model [7].

(ii) Important configuration interaction of the $4s4f$-$4p4d$ and $4p4f$-$4d^2$ kind was found [1]. Since configuration interaction was not taken into account in the SOSA model, identification of individual lines superimposed on the pseudocontinuum was discarded in Ref. [1]. Nevertheless, the major features of the $3d$-$4f$ pseudocontinuum could be analyzed, and the conclusion was reached that the different peaks in the experimental spectrum correspond to $3d$-$4f$ transitions in the successive lower-ionization states. This was confirmed by the analysis of $\Delta n > 1$ transitions [8–11] where these discrepancies were found to be negligible. It must be stressed that the global effect of configuration interaction on the intensity distribution of unresolved transition arrays [12] is now also well understood [13]. However, no studies have been performed on the global effect of configuration mixing on the structure of the spin-orbit split arrays. Since this effect is crucial to the understanding of the details of the $3d$-$4f$ emission pattern as it appears, for example, in the spectrum emitted by the tantalum laser-produced plasma of Fig. 1, a more detailed study of this effect has been undertaken.

II. THEORY

The wavelengths and gf values of the transitions were computed using the RELAC code implemented on the Naval Research Laboratory Cray computer. Parametric potential optimization was performed using the variational criterion on the average energy of the excited configuration. A correcting shift (see, for example, Ref. [11]) was used for the ground-state energy on the final computation. The same method was used in many previous works (Refs. [1] and [10], for example).

III. EFFECT OF CONFIGURATION MIXING

A. Global effect

The global effect of the configuration mixing on $3d$-$4f$ transitions will first be shown in a qualitative way in four different transitions pertaining to three ionic states. In each case the effect of the configuration mixing is shown by comparing the results of the *ab initio* intermediate coupling computation in the form of theoretical spectra. In these theoretical spectra, the height of each line is proportional to gA, g being the statistical weight of the upper level and A the transition probability. The first theoretical spectrum shows the results of the computation before introduction of the mixing. The second (and, in Fig. 2, the third spectrum also) shows the results of the computation including the perturbing configuration. All the computations have been performed for highly ionized tantalum.

1. Ta XLIII

The results of the computations for Ga-like Ta XLIII are displayed in Figs. 2(a)–2(c). Figure 2(a) gives the results of the single configuration $3d^{10}4s^24p$-$3d^94s^24p4f$

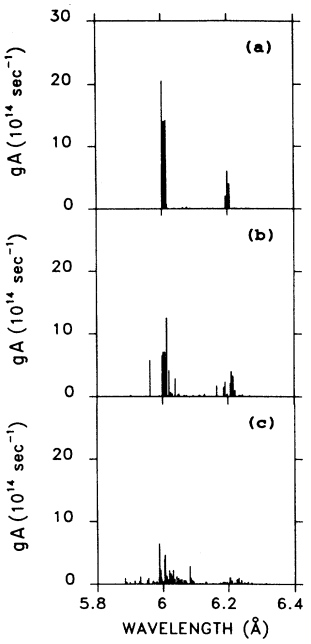

FIG. 2. Transitions in Ga-like Ta XLIII: (a) $3d^{10}4s^24p$-$3d^94s^24p4f$; (b) $3d^{10}4s^24p$-$3d^9(4s^24p4f+4s^24d^2)$; (c) $3d^{10}4s^24p$-$3d^9(4s^24p4f+4s^24d^2+4s4p^24d)$.

computation, whereas Fig. 2(b) includes mixing of the upper configuration with $3d^94s^24d^2$. Figure 2(c) displays the results of the $3d^{10}4s^24p$-$3d^9(4s^24p4f+4s^24d^2+4s4p^24d)$ computation, allowing mixing through

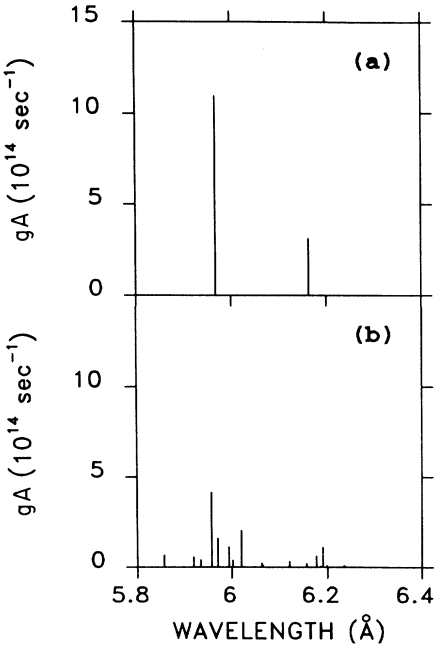

FIG. 3. Transitions in Zn-like Ta XLIV. (a) $3d^{10}4s^2$-$3d^94s^24f$; (b) $3d^{10}4s^2$-$3d^9(4s^24f+4s4p4d)$.

$4s4f$-$4p4d$ and $4p4f$-$4d^2$ interaction. The third configuration adds 452 levels to the 113 levels already present in the second case.

2. Ta XLIV

In the Zn I-like isoelectronic sequence the $3d^{10}4s^2$-$3d^9 4s^2 4f$ transition has been computed [Fig. 3(a)] and the effect of the mixing of the upper configuration with the $3d^9 4s4p4d$ configuration is shown [Fig. 3(b)]. It must be pointed out that the $4s^2 4f$-$4s4p4d$ mixing has already been observed for $\Delta n=0$ transitions in the Ga I-like sequence [14]. The single-configuration computation gives, in analogy with the Ni-like transition, three lines corresponding to each of the three SOSA subarrays. Since the third line at the longest wavelength has a gA value smaller than the gA value of the two other lines by three orders of magnitude, only the two strongest lines are visible. The width of each of these subarrays is, of course, $\Delta\lambda=0$. This is the width listed for this transition in Ref. [15] (see Table I therein). The computed transition including configuration mixing shows now many lines in the 5.9–6.0 Å-wavelength range, and thus the actual subarrays have finite width.

3. Ta XLV

For the Cu-like $3d^{10}4s$-$3d^9 4s4f$ transition, mixing of the upper configuration with $3d^9 4p4d$ was introduced into the computation, and the results are displayed in Figs. 4(a) and 4(b). The importance of this configuration mixing has been pointed out previously [1]. For the $\Delta n=0$ transitions, the strong $4s4f$-$4p4d$ interaction has also been studied in the Zn I sequence [16]. The Cu-like $3d^{10}4p$-$3d^9 4p4f$ transition has also been computed and the effect of the configuration mixing with the $3d^9 4d^2$ configuration has been calculated. The results are displayed in Figs. 5(a) and 5(b).

The following conclusions can be drawn from Figs. 2–5.

(i) In each case, the general structure of three subarrays is not changed.

(ii) The subarray widths are much larger when configuration mixing is introduced.

(iii) Line intensities are smaller in the case of configuration mixing because this intensity is shared between many more lines.

(iv) It seems that the mean wavelengths of the subarrays are not changed.

To express these facts in a more quantitative way, the line-strength-weighted mean wavelengths $\bar{\lambda}$ and spectral widths $\Delta\lambda$ of the arrays were calculated using the computed data for individual lines (unlike the UTA or SOSA models). $\bar{\lambda}$ and $\Delta\lambda$ are defined by the following equations:

$$\bar{\lambda}=\frac{\sum_{i,j} g_i A_{ij}\lambda_{ij}}{\sum_{i,j} g_i A_{ij}}, \quad \Delta\lambda=\left[\frac{\sum_{i,j}(\bar{\lambda}-\lambda_{ij})^2 g_i A_{ij}}{\sum_{i,j} g_i A_{ij}}\right]^{1/2},$$

where λ_{ij} is the wavelength, A_{ij} the Einstein coefficient

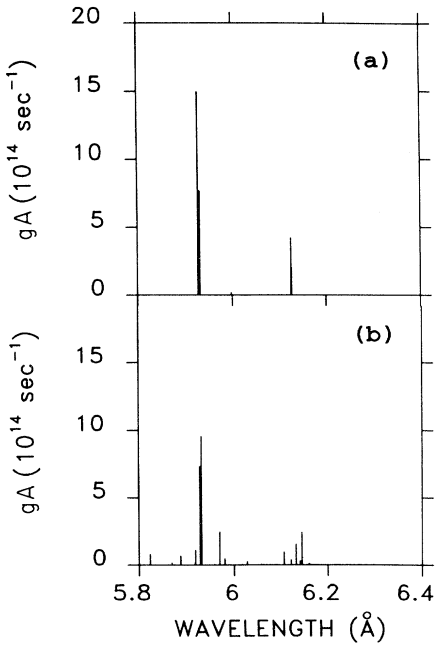

FIG. 4. Transitions in Cu-like Ta XLV with the $4s$ spectator electron. (a) $3d^{10}4s$-$3d^9 4s4f$; (b) $3d^{10}4s$-$3d^9(4s4f+4p4d)$.

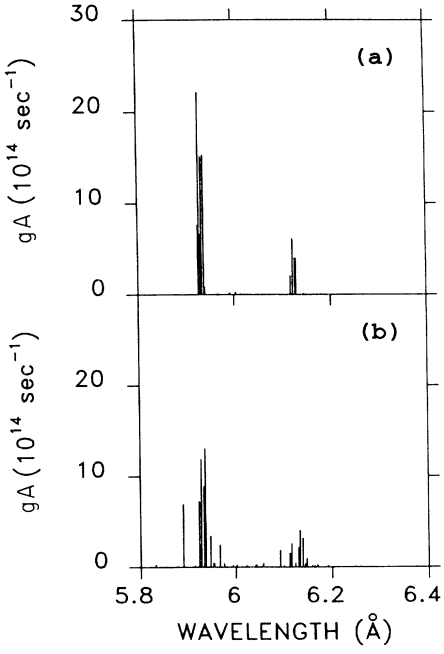

FIG. 5. Transitions in Cu-like Ta XLV with the $4p$ spectator electron. (a) $3d^{10}4p$-$3d^9 4p4f$; (b) $3d^{10}4p$-$3d^9(4p4f+4d^2)$.

of the computed transition line, and g_i is the statistical weight of the upper level. Only those lines in the selected wavelength range r are included in the summation. $\bar{\lambda}$ represents the line-strength-weighted mean wavelength and $\Delta\lambda$ the spectral width of the subarrays (these results are equivalent to the results of the SOSA model for the single-configuration calculations). The weighted mean wavelengths and spectral widths obtained are given in Table I for the three isoelectronic sequences considered. In each case, the mean wavelength and spectral width have been computed for lines in three different wavelength ranges, r_1, r_2, and r_3. Here λ_1, λ_2, and λ_3 are the mean wavelengths of the three SOSA subarrays corresponding to $3d_{3/2}$-$4f_{5/2}$, $3d_{5/2}$-$4f_{7/2}$, and $3d_{5/2}$-$4f_{5/2}$ transitions, respectively, and the three wavelength ranges were chosen as follows: the first range (r_1) from $\lambda=0$ to $\lambda=0.5\,(\lambda_1+\lambda_2)$, the second ($r_2$) from $\lambda=0.5\,(\lambda_1+\lambda_2)$ to $\lambda=0.5\,(\lambda_2+\lambda_3)$, the third ($r_3$) from $\lambda=0.5\,(\lambda_2+\lambda_3)$ to $\lambda=\infty$. These three wavelength ranges correspond to the maximum spread of each of the three SOSA subarrays. From Table I, the very significant effect of configuration mixing on the SOSA width is evident. Since this kind of configuration mixing is not included in the SOSA model at the present time, the results of the SOSA computations, like those displayed in Table I of Ref. [15], should be taken with caution as far as the width of the subarray is concerned. Of course, in many other cases the configuration interaction could be negligible. For example, it can be anticipated that for a transition like $3d^{10}4f$-$3d^{9}4f^{2}$ or $3d^{10}4d$-$3d^{9}4d4f$ the configuration interaction of the upper levels with the configuration of the $3d^{9}4l4l'$ complex may be less important because there is no near-degenerate configuration in the same complex. This has not been investigated in the present work. However, for all the transitions of the kind $3d^{10}4s^{k}4p^{m}$-$3d^{9}4s^{k}4p^{m}4f$ ($k=1,2$ and $m=1$ to 5), configuration mixing of the upper configuration with $3d^{9}4s^{k}4p^{m-1}4d^{2}$ and $3d^{9}4s^{k-1}4p^{m+1}4d$ is crucial and should be taken into account for any estimation of the SOSA width. On the other hand, it appears from Table I that the mean wavelength of each of the subarrays is almost not changed. This interesting conclusion was not generalized to other transition arrays because of the complexity of the computations involved.

B. Line identification

In view of the effect of configuration interaction, previous works where these effects were not taken into account are reviewed. First, in Ref. [1], extensive use of the SOSA model was made. The conclusion of Klapisch *et al.* [1] was that the band structure ("pseudocontinuum") in the long-wavelength side of the resonance Ni-like transition arises from the contribution of the different ionization states, whereas for each ionization state several transitions involving different spectator configurations can be involved. Since this conclusion relies essentially on the mean wavelength and not on the width of the computed SOSA subarrays, this conclusion is not affected by the present work. As a conclusion, the authors wrote: "Other reasons (which contribute to the broadening of each

TABLE I. Mean wavelength and width of tantalum Cu-, Zn-, and Ga-like $3d$-$4f$ transition subarrays calculated from the results of full intermediate-coupling line computation for lines in three different wavelength ranges, r_1, r_2, and r_3.

Ion	Transition	r_1 (Å)	$\bar{\lambda}_1$ (Å)	$\Delta\lambda$ (mÅ)	r_2 (Å)	$\bar{\lambda}_2$ (Å)	$\Delta\lambda$ (mÅ)	r_3 (Å)	$\bar{\lambda}_3$ (Å)	$\Delta\lambda_3$ (mÅ)
Ta XLV	$3d^{10}4s$-$3d^{9}4s4f$	[0,6.036]	5.9315	6.5	[6.036,6.169]	6.1260	0.8	[6.169,∞]	6.1970	14.8
	$3d^{10}4s$-$3d^{9}(4s4f+4p4d)$		5.9320	28.7		6.1324	16.7		6.3322	79.1
	$3d^{10}4p$-$3d^{9}4p4f$		5.9315	9.0		6.1261	5.0		6.1959	39.9
	$3d^{10}4p$-$3d^{9}(4p4f+4d^{2})$		5.9304	21.6		6.1224	23.3		6.1924	29.8
Ta XLIV	$3d^{10}4s^{2}$-$3d^{9}4s^{2}4f$	[0,6.070]	5.9682	0.0	[6.070,6.206]	6.1634	0.0	[6.206,∞]	6.2478	0.0
	$3d^{10}4s^{2}$-$3d^{9}(4s^{2}4f+4s4p4d)$		5.9708	42.5		6.1732	25.4		6.2706	70.8
Ta XLIII	$3d^{10}4s^{2}4p$-$3d^{9}4s^{2}4p4f$	[0,6.107]	6.0078	9.2	[6.107,6.246]	6.2029	5.2	[6.246,∞]	6.2715	39.3
	$3d^{10}4s^{2}4p$-$3d^{9}4s^{2}(4p4f+4d^{2})$		6.0066	22.2		6.1996	25.0		6.2790	29.7
	$3d^{10}4s^{2}4p$-$3d^{9}(4s^{2}4p4f$ $+4s^{2}4d^{2}+4s4p^{2}4d)$		6.0085	44.9		6.1998	33.9		6.2897	58.8

band) may be configuration interactions, which shift the different transitions arrays differently, thus making the true array wider." In light of the present work, it seems that the spreading of the array is the main consequence of the configuration mixing.

Further analysis of the $3d$-$4f$ pseudocontinuum appearing in the laser-produced-plasma Ta spectrum and based on the SOSA model was performed by Bauche-Arnoult *et al.* [15]. In the latter work, an interpretation of the successive peaks appearing on the long-wavelength side of the Ni-like $3d^{10}$-$3d^9_{3/2}4f_{5/2}(J=1)$ line at $\lambda=5.907$ Å was given as a superposition of two "grids" of arrays. The first grid was composed of transitions of the kind $3d^{10}4l^i4l'^j\ldots$-$3d^94l^i4l'^j\ldots4f$, the different $m=i+j+\cdots$ corresponding to the successive lower-ionization states—essentially the same interpretation as that of Klapisch *et al.* [1]. The Ni-like line and the successive peaks of this first grid have been labeled $A,B,C\ldots$ on the spectrum of Fig. 1, following the labeling of Bauche *et al.* in Fig. 2 of Ref. [15]. The second grid was composed of transitions of the kind $3d^{10}4l^i4l'^j\ldots5l^*$-$3d^94l^i4l'^j\ldots5l^*4f$, with $i+j+\cdots=m-1$, i.e., like the first grid but replacing one of the $n=4$ spectator electrons by a $5l^*$ electron. The peaks of this second grid have been labeled in Fig. 1, as $b,c,d,\ldots$, as in Ref. [15]. Each peak of the second grid was found to be shifted towards shorter wavelengths by about 27 mÅ relative to the corresponding peak of the first grid. This allowed the authors to identify, in particular, a line appearing at $\lambda=5.919$ Å (labeled b) on the long-wavelength side of the Ni-like line as a Cu-like transition of the second grid. Also, a feature appearing at $\lambda=5.957$ Å (c), on the long-wavelength side of the Cu-like transition B of the first grid (at $\lambda=5.946$ Å) was identified as a Zn-like transition of the second grid. Since all the upper configurations of the transitions of the second grid are above ionization threshold, doubly excited, and cannot be reached by electron-impact excitation at the electron density and temperature involved, the conclusion was reached that these lines are satellites resulting from dielectronic recombination. The identification of the different peaks was made using the SOSA model without configuration mixing. This was further supported by an average model for dielectronic recombination of the Ni-like ion into the Cu-like ion. The present work now deals with the identification of individual lines in the experimental spectrum in view of the effect of configuration mixing as explained above. In particular we address the spectroscopic identification of the lines b and c of the second grid at $\lambda=5.919$ and 5.957 Å.

It must be stressed that relying on the SOSA single-configuration computation only, the identification of line b as a satellite with a $5l$ electron is particularly attractive. Indeed, owing to the fact that this rather intense line lies outside the range of any of the $3d$-$4f$ transitions of the Cu-like and lower-ionization states as derived from the calculated SOSA width, a possible alternative identification of this line would be difficult.

However, the present computations show that because of the configuration mixing, some resonance Cu- and Zn-like inner-shell excited transitions have wavelengths very close to the b and c lines, whose origin is attributed in Ref. [15] to dielectronic recombination. This is shown in Tables II and III where detailed results of the computation of the $3d^{10}4s$-$3d^94s4f$ transition in Cu-like Ta XLV and of the $3d^{10}4s^2$-$3d^94s^24f$ transition in Zn-like Ta XLIV are given. In each table the results of the computation before introduction of the perturbating configuration is given for comparison [Tables II(a) and III(a)]. The final results including the mixing are given in Table II(b) [$3d^{10}4s$-$3d^9(4s4f+4p4d)$] and III(b) [$3s^{10}4s^2$-$3d^9(4s^24f+4s4p4d)$], respectively. In these tables, the first column gives the spectroscopic designation of the upper level in a shortened jj notation. The J value of the intermediate coupling of the successive open shells is given in parentheses. The total J of the upper level follows the

TABLE II. Ta XLV $3d^{10}4s$-$3d^94s4f$ transitions. Only transitions with $gf>0.5$ are listed. The eigenvectors are given in a shortened jj notation where $l_+=l_{j=l+1/2}$, and $l_-=l_{j=l-1/2}$ (see text). For example $[3d^9_-4s(1)4f_-]_{3/2}$ means that the hole in the $3d$ shell with $j=3/2$ has been coupled with the $j=\frac{1}{2}$ of the $4s$ electron to give the intermediate $J^*=1$, which, in turn, has been coupled to the $j=\frac{5}{2}$ of the $4f$ outer electron to give the total $J=\frac{3}{2}$ of the level. The number in front of the level designation is the square of the eigenvector, the sign showing the relative phase of the components.

Upper-level composition	λ (Å)	gf
(a) Single-configuration computation		
$0.48[3d^9_-4s(1)4f_-]_{3/2}+0.36[3d^9_-4s(2)4f_-]_{3/2}$	5.929	8.08
$+0.84[3d^9_-4s(2)4f_-]_{1/2}$	5.933	4.15
$+0.42[3d^9_+4s(2)4f_+]_{3/2}+0.32[3d^9_+4s(3)4f_+]_{3/2}$	6.125	2.48
$+0.79[3d^9_+4s(2)4f_+]_{1/2}$	6.127	1.16
(b) Including configuration mixing with $3d^94p4d$		
$+0.42[3d^9_-4p_+(3)4d_+]_{3/2}-0.31[3d^9_-4p_+(1)4d_+]_{3/2}$	5.920	0.65
$+0.78[3d^9_-4s(2)4f_-]_{1/2}$	5.929	3.92
$-0.32[3d^9_-4s(1)4f_-]_{3/2}-0.21[3d^9_-4s(2)4f_-]_{3/2}$	5.932	5.17
$+0.50[3d^9_-4p_+(1)4d_-]_{3/2}-0.23[3d^9_-4p_+(3)4d_-]_{3/2}+0.09[3d^9_-4s(2)4f_-]_{3/2}$	5.970	1.31
$+0.13[3d^9_+4p_+(2)4d_+]_{3/2}+0.30[3d^9_+4p_+(1)4d_+]_{3/2}+0.15[3d^9_+4s(2)4f_+]_{3/2}$	6.106	0.56
$+0.52[3d^9_+4s(3)4f_+]_{1/2}$	6.131	0.88
$-0.30[3d^9_+4s(2)4f_+]_{3/2}-0.14[3d^9_+4s(3)4f_+]_{3/2}+0.23[3d^9_+4p_+(1)4d_-]_{3/2}$	6.144	1.39

TABLE III. Ta XLIV $3d^{10}4s^2$-$3d^9 4s^2 4f$ transitions.

Upper-level composition	λ (Å)	gf
(a) Single-configuration computation		
$0.85(3d^9_- 4s^2 4f_-)$	5.969	5.84
$0.77(3d^9_+ 4s^2 4f_+)$	6.163	1.79
$0.91(3d^9_+ 4s^2 4f_-)$	6.247	0.005
(b) Including configuration mixing with $3d^9 4s 4p 4d$ ($gf \geq 0.3$)		
$-0.18[3d^9_- 4s(1)4p_+(5/2)4d_-]+0.18[3d^9_- 4s(2)4p_+(3/2)4d_-]+0.13[3d^9_- 4s(2)4p_+(5/2)4d_-]$	5.857	0.35
$+0.63[3d^9_- 4s(2)4p_+(3/2)4d_+]-0.15[3d^9_- 4s(1)4p_+(3/2)4d_+]+0.06[3d^9_- 4s^2 4f_-]$	5.919	0.31
$+0.34[3d^9_- 4s^2 4f_-]+0.16[3d^9_- 4s(2)4p_+(1/2)4d_-]+0.19[3d^9_- 4s(2)4p_+(7/2)4d_+]$	5.958	2.21
$+0.13[3d^9_- 4s^2 4f_-]+0.20[3d^9_- 4s(2)4p_+(3/2)4d_-]-0.23[3d^9_- 4s(2)4p_+(7/2)4d_+]$	5.971	0.86
$+0.23[3d^9_- 4s(2)4p_+(3/2)4d_-]+0.13[3d^9_- 4s(2)4p_+(7/2)4d_+]+0.14[3d^9_- 4s(2)4p_+(5/2)4d_+]$	5.994	0.61
$+0.44[3d^9_- 4s(2)4p_+(1/2)4d_-]-0.11[3d^9_{3/2}4s^2 4f_{5/2}]+0.08[3d^9_- 4s(1)4p_+(5/2)4d_-]$	6.021	1.11
$+0.30[3d^9_+ 4s(2)4p_+(3/2)4d_+]+0.16[3d^9_{3/2}4s^2 4f_{7/2}]+0.14[3d^9_- 4s(2)4p_+(5/2)4d_-]$	6.176	0.36
$+0.29[3d^9_+ 4s^2 4f_+]-0.12[3d^9_- 4s(2)4p_-(5/2)4d_-]-0.10[3d^9_+ 4s(3)4p_+(3/2)4d_-]$	6.190	0.64

level designation is the square of the eigenvector, the sign showing the relative phase of the components. The lower level is $3d^{10}4s$ ($J=\frac{1}{2}$) for Table II and $3d^{10}4s^2$ ($J=0$) for Table III. The next column gives the computed wavelength (in angstroms) and the gf values. As can be seen from Tables II(b) and III(b), possible alternative identification for the line b at the measured wavelength $\lambda=5.919$ Å (Ref. [15], Table III) is the Cu-like $3d^{10}4s$-$3d^9 4s 4f$ line at the computed wavelength $\lambda=5.920$ Å ($gf=0.65$) blended with the Zn-like line at 5.919 Å ($gf=0.31$). Moreover, an alternative identification for the line c of the second grid at $\lambda=5.957$ Å is the Zn-like $3d^{10}4s^2$-$3d^9 4s^2 4f$ line at the computed $\lambda=5.958$ Å ($gf=2.21$). And the yet unidentified line labeled a in Fig. 1, which has a measured wavelength $\lambda=5.855$ Å, is identified as the Zn-like line at a computed wavelength $\lambda=5.857$ Å ($gf=0.35$). This shows clearly that inner-shell excited transitions can contribute to the intensity of lines b and c.

IV. DISCUSSION

A. Accuracy of the computations

Definitive identification of the spectral lines for the kind of spectra that are dealt with in the present work has to rely on isoelectronic regularity. Indeed, neither the accuracy of the computed $3d$-$4f$ transition nor the experimental spectral resolution allows definitive identification based on the spectrum of one element. The 2-mÅ agreement between the measured and calculated wavelength of the transitions as reported in the previous section should be considered as rather fortuitous, the usual agreement for this kind of transition being in general of the order of 5 mÅ (Ref. [18]). The remaining discrepancies arise from many factors. The most important are residual configuration interactions not taken into account in the computation [for example, in the case of $3d^{10}4s^2$-$3d^9(4s^2 4f+4s4p4d)$, the blending of the upper configurations with $3d^9 4p^3$], overestimation of the exchange integral (which is particularly important for the Ni-like $3d^{10}$-$3d^9_{3/2}4f_{5/3}$ and satellite transitions), and the central field approximation. In the case of the SOSA model computations the interaction between the relativistic subconfigurations that has been neglected is one more factor. Here it is worth mentioning that in Ref. [15] the wavelengths of the $3d_{3/2}$-$4f_{5/2}$ transitions (calculated using the SOSA model) have been shifted by 0.015 Å to fit the experimental values. The configuration interaction between the $3d_j^9 4f_{j'}$ relativistic subconfigurations has been invoked by the authors to justify this shift. For example, for the $3d^{10}4s^2$-$3d^9_{3/2}4s^2 4f_{5/2}$ Zn-like transition, the SOSA result, $\lambda=6.000$ Å, has been shifted to 5.985 Å

TABLE IV. Identification of the Zn-like a line along the isoelectronic sequence.

	Theory			Experiment	
Ion	Upper-level composition	λ (Å)	gf	λ (Å)	λ_{expt}-λ_{theor} (mÅ)
Tm XL	$-0.15\alpha+0.11\beta+0.16\gamma+0.11\delta+0.10\epsilon$	6.881	0.75	6.870	−11
Yb XLI	$-0.15\alpha+0.12\beta+0.16\gamma+0.12\delta+0.08\epsilon$	6.603	0.62	6.592	−11
Hf XLIII	$-0.17\alpha+0.12\beta+0.17\gamma+0.12\delta+0.06\epsilon$	6.091	0.42	6.079	−12
Ta XLIV	$-0.18\alpha+0.12\beta+0.18\gamma+0.13\delta+0.05\epsilon$	5.857	0.35	5.855	−2
$\alpha=[3d^9_- 4s(1)4p_+(5/2)4d_-]J=1$		$\beta=[3d^9_- 4s(2)4p_+(1/2)4d_-]J=1$		$\gamma=[3d^9_- 4s(2)4p_+(3/2)4d_-]J=1$	
$\delta=[3d^9_- 4s(2)4p_+(5/2)4d_-]J=1$		$\epsilon=[3d^9_- 4s^2 4f_-]J=1$			

TABLE V. Difference between measured and calculated wavelength of the Ni-like $3d^{10}$-$3d^{9}_{3/2}4f_{5/2}$ transition.

Ion	λ (Å) (theory)	λ (Å) (experiment)	λ_{expt}-λ_{theor} (mÅ)
Tm XL	6.885[a]	6.890[a]	5
Yb XLI	6.615[a]	6.620[a]	5
Hf XLIII	6.122[b]	6.125[b]	3
Ta XLIV	5.895[b]	5.907[b]	12
W XLVII	5.682[b]	5.689[b]	7
Re XLVIII	5.479[b]	5.484[b]	5

[a]Reference [17].
[b]Reference [18].

(Tables I and III in Ref. [15]) to fit the experiment wavelength of the peak at a measured wavelength λ=5.983 Å. However, the above-mentioned interaction would have shifted the SOSA result to λ=5.969 Å, which is the value given in Table III(a) differing from the SOSA computation only by the introduction of this relativistic subconfiguration mixing. It is the other factors, as explained above, which account for the remaining discrepancy of 0.014 mÅ.

B. Identification along the isoelectronic sequence

In view of the precision of the theoretical computation and of the experimental spectral resolution as obtained in Refs. [1] and [15], it seems difficult to confirm the identification of lines *b* and *c* along the isoelectronic sequence. Predictions for the wavelength of *b* and *c*, following either identification as inner-shell excited or from dielectronic recombination, are very smooth along the isoelectronic sequence, and these lines remain blended with the strong Ni-like line and satellite Cu-like SOSA in the isoelectronic spectrum of neighboring atoms. Line *a* however, is a good candidate for the confirmation of the validity of the present calculations since this line is well isolated and appears in the spectra of Tm, Yb, and Hf as reported in Ref. [1]. Table IV gives the results of the computation and the measured wavelength of this line. The overall agreement between theory and experiment is good. The discrepancy between theory and observation is about 11 mÅ for Tm XL, Yb XLI, and Hf XLIII, and 2 mÅ for Ta XLIV. This irregularity should not dismiss the identification of line *a* as a Zn-like transition since the same trend is observed when comparing measured and calculated wavelengths of the very close $3d_{3/2}$-$4f_{5/2}$ strong Ni-like line as reported in Refs. [17] and [18] (see Table V). This is probably due to a wavelength shift of the experimental tantalum spectrum.

V. CONCLUSION

In the present work it is shown using *ab initio* computation that configuration mixing has to be taken into account in the computation of the mean wavelength and width of the $3d$-$4f$ arrays in Ga I, Zn- and Cu-like tantalum. These configuration interactions are strong because they are in a quasidegenerate complex. Because of the mixing, the first two lines of the "grid" interpreted as dielectronic satellites with one $5l$ electron in Ref. [15] have an alternative interpretation as inner-shell resonance transitions in the Cu I and Zn I ionization states or at the very least as a superposition of two transitions. We caution the user of these lines as a diagnostic tool for a recombining plasma to be aware of the possible contribution of inner-shell excitation to the line intensities. This conclusion does not involve any assumption about plasma conditions.

Finally, in the case of $3d$-$5f,6f$ transitions [8,9] the importance of configuration mixing might be much smaller, and this fact can explain the very good agreement between the predictions of the array width by the SOSA model and the experimental observations.

ACKNOWLEDGMENTS

One of the authors (P.M.) is grateful to the Solar Terrestrial Relationships Branch of the E. O. Hulburt Center for Space Research at the Naval Research Laboratory for hospitality during his stay. The authors would like to thank C. Bauche-Arnoult and J. Bauche for reading the manuscript and making valuable comments prior to publication. This work was supported by the Strategic Defense Initiative Organization under Contract No. N001490WX15516.

*Permanent address: Racah Institute of Physics, Hebrew University, 91904 Jerusalem, Israel.

[1] M. Klapisch, P. Mandelbaum, A. Zigler, C. Bauche-Arnoult, and J. Bauche, Phys. Scr. **34**, 51 (1986).
[2] J. F. Wyart, A. M. Van Kleef, A. N. Ryabtsev, and Y. N. Joshi, Phys. Scr. **29**, 319 (1984).
[3] M. Busquet, D. Pain, J. Bauche, and E. Luc-Koenig, Phys. Scr. **31**, 137 (1985).

[4] M. Klapisch, J. L. Schwob, B. S. Fraenkel, and J. Oreg, J. Opt. Soc. Am. **67**, 148 (1977).
[5] C. Bauche-Arnoult, J. Bauche, and M. Klapisch, Phys. Rev. A **31**, 2248 (1985).
[6] C. Bauche-Arnoult, J. Bauche, and M. Klapisch, Phys. Rev. A **20**, 2424 (1979); J. Bauche, C. Bauche-Arnoult, and M. Klapisch, Adv. At. Mol. Phys. **27**, 131 (1987).
[7] J. Bauche, C. Bauche-Arnoult, and M. Klapisch, J. Phys. B **24**, 1 (1991).
[8] P. Audebert, J. C. Gauthier, J. P. Geindre, C. Chenais-Popovics, C. Bauche-Arnoult, J. Bauche, M. Klapisch, E. Luc-Koenig, and J. F. Wyart, Phys. Rev. A **32**, 409 (1985).
[9] C. Bauche-Arnoult, E. Luc-Koenig, J. F. Wyart, J. P. Geindre, P. Audebert, P. Monier, J. C. Gauthier, and C. Chenais-Popovics, Phys. Rev. A **33**, 791 (1986).
[10] A. Zigler, M. Klapisch, and P. Mandelbaum, Phys. Lett. A **117**, 31 (1986).
[11] N. Tragin, J. P. Geindre, P. Monier, J. C. Gauthier, C. Chenais-Popovics, J. F. Wyart, and C. Bauche-Arnoult, Phys. Scr. **37**, 72 (1988).
[12] P. Mandelbaum, M. Finkenthal, J. L. Schwob, and M. Klapisch, Phys. Rev. A **35**, 5051 (1987).
[13] J. Bauche, C. Bauche-Arnoult, M. Klapisch, P. Mandelbaum, and J. L. Schwob, J. Phys. B **20**, 1443 (1987).
[14] U. Litzen and A. Hansson, Phys. Scr. **40**, 463 (1989).
[15] C. Bauche-Arnoult, J. Bauche, E. Luc-Koenig, R. M. More, J. F. Wyart, C. Chenais-Popovics, J. C. Gauthier, J. P. Geindre, and N. Tragin, Phys. Rev. A **39**, 1053 (1989).
[16] U. Litzen and J. Reader, Phys. Scr. **39**, 73 (1989).
[17] A. Zigler, H. Zmora, N. Spector, M. Klapisch, J. L. Schwob, and A. Bar-Shalom, J. Opt. Soc. Am. **70**, 129 (1980).
[18] M. Klapisch, A. Bar-Shalom, P. Mandelbaum, J. L. Schwob, A. Zigler, H. Zmora, and S. Jackel, Phys. Lett. **79A**, 67 (1980).